 https://doi.org/10.3311/PPtr.41190

Periodica Polytechnica Transportation Engineering, 54(1), pp. 88–104, 2026

Validation of a Small UAV Dynamic Model Using CFD and Flight Test Data

Eries Bagita Jayanti[1*], Novita Atmasari[1], Angga Septiyana[1,2], Ardian Rizaldi[1,3], Try Kusuma Wardana[1], Aries Asrianto Ramadian[1], Hidayati Mardikasari[1], Hartono Hartono[1]

[1] Research Center of Aeronautics Technology, National Research and Innovation Agency, KS Jacob Salatun, Rumpin, Bogor, West Java 16350, Indonesia
[2] Mechanical Engineering, Faculty of Engineering, Universitas Indonesia, Depok, West Java Indonesia
[3] Aerospace Engineering, Graduate School of Mechanical and Aerospace Engineering, Gyeongsang National University, Jinju, Gyeongsangnam-do, Republic of Korea
[*] Corresponding author, e-mail: erie002@brin.go.id

Received: 03 June 2025, Accepted: 22 September 2025, Published online: 14 November 2025

Abstract

Fixed-wing Unmanned Aerial Vehicles (UAV) are increasingly utilized in various missions requiring stable and responsive performance. Accurate dynamic models are essential to ensure effective UAV control. This study presents the development and validation of a 6-DOF UAV dynamic model, constructed using aerodynamic data derived from Computational Fluid Dynamics (CFD) simulations. The model integrates aerodynamics, weight, and thrust. To validate the model, three sets of flight test data were collected. The dataset showed the most consistent trends. The longitudinal, phugoid and short-period modes were successfully executed. However, residual oscillations in pitch angle and forward speed responses suggest the need to re-evaluate pitch-related aerodynamic coefficients and include CDu to the model. Despite these oscillations, pitch angle and pitch rate exhibited the lowest Mean Absolute Error (MAE) values when compared to flight data, indicating strong agreement in trend and amplitude. In contrast, forward speed showed the highest MAE due to discrepancies in initial conditions. For lateral/directional modes, characteristic responses such as roll subsidence, spiral, and Dutch roll were accurately reproduced. Yaw rate achieved the best fit, while yaw angle had the largest MAE due to range differences between simulation and flight test data. The differences between simulation results and flight test data are mainly due to the inaccuracy of aerodynamic coefficients in some parameters, simplifying assumptions in CFD simulations, as well as differences in initial conditions. Overall, the results demonstrate that the CFD-derived aerodynamic model, when validated against flight test data, can reliably represent the actual dynamic behaviour of a UAV.

Keywords

unmanned aerial vehicle, computational fluid dynamics, flight test, dynamic model, validation

1 Introduction

Unmanned aerial vehicle (UAV), as an emerging technology, offers a versatile and cost-effective alternative to conventional aircraft. There are two platforms of UAVs available on the market: fixed-wing UAVs and rotary-wing UAVs. Fixed-wing UAVs provide significantly greater range, higher energy efficiency, and greater payload capacity compared to rotary-wing UAVs (Mahachi et al., 2022). They are employed for various missions, particularly in fields such as aerial mapping, shipping and delivery, agricultural monitoring, reconnaissance, and surveillance (Paz et al., 2021). Many of these missions necessitate a stable UAV to ensure precise control and reliable performance. Achieving stability in UAV design should begin with developing an accurate dynamic model. The UAV dynamic model is a mathematical representation that characterizes the aircraft's response to aerodynamic forces and moments. The accuracy of this model is essential to ensure that the UAV can be effectively controlled and remains responsive in a diverse range of flight conditions. However, the development of dynamic models often encounters significant technical hurdles, such as limited aerodynamic data obtained from simulations or experiments, as well as the lack of validation based on flight test data (Benyamen et al., 2024). Without an adequate validation process, dynamic models may generate inaccurate

Cite this article as: Jayanti, E. B., Atmasari, N., Septiyana, A., Rizaldi, A., Wardana, T. K., Ramadian, A. A., Mardikasari, H., Hartono, H. (2026) "Validation of a Small UAV Dynamic Model Using CFD and Flight Test Data", Periodica Polytechnica Transportation Engineering, 54(1), pp. 88–104.
https://doi.org/10.3311/PPtr.41190

simulation results, thereby hampering UAV performance optimization in executing its mission (Fatima et al., 2023).

Stability is a crucial factor in control. With an accurate model, an appropriate control system can be designed (Priyambodo and Majid, 2021). Stability and control are closely related concepts that influence the aircraft's movements. A highly stable aircraft tends to be difficult to manoeuvre, whereas one with minimal stability is easier to control. However, reduced stability can negatively impact flight performance, making the aircraft harder to operate and less reliable in flight (Federal Aviation Administrative, 2021).

In practice, there are frequently used methods to develop the dynamic model: computational methods and experimental methods, including wind tunnel testing and flight testing (Farhadi et al., 2018; Wu et al., 2023). Computational methods, such as CFD, are widely used to analyse the aerodynamic behaviour of UAVs and can yield the highest level of accuracy (Consentino, 2007). This method is cost-effective and practical. It also can be performed repeatedly under different conditions within a relatively short period of time (Mateen et al., 2024). Meanwhile, wind tunnel testing requires specialized equipment that is not readily available in many laboratories. The high cost of testing must also be taken into consideration (Aljuhaishi et al., 2024). Wind tunnel testing is conducted in a controlled environment, conversely, flight testing is performed in an uncontrolled environment (Jeong et al., 2024). Therefore, flight test data are susceptible to noise from exogenous variables, such as wind, which is often absent in wind tunnel tests (Jeong et al., 2024). In addition, planning and executing flight tests can be expensive, time-consuming, and labour-intensive (Sun et al., 2022), making it a challenging validation method.

Nevertheless, for the model to be considered having satisfactory accuracy, computational data must be validated against flight test data to ensure consistency with actual conditions. The validation of CFD simulations against experimental data may reveal discrepancies that could affect both UAV performance and behaviour. Prior numerous studies have evaluated these modelling and validation approaches. Gryte et al. (2018) conducted a study to establish an accurate model by comparing numerical design tools and wind tunnel testing, focusing on the Skywalker X8 fixed-wing unmanned aerial vehicle as a case study. Similarly, Elbedewy et al. (2021) proposed a combination of approaches that integrates both computational and experimental techniques to develop a dynamic model of a Cessna UAV. Wu et al. (2023) also compared numerical simulations with airborne flight tests under the same conditions. However, a shortfall of this research is that wind tunnel testing did not generate dynamic stability derivatives. Integrating wind tunnel testing and flight experiments to develop an aerodynamic model has been well-documented by multiple researchers (Reinhardt et al., 2022; Pusztai et al., 2024).

Overall, it is of fundamental importance to evaluate the accuracy of the model by comparing software-generated data with experimental data from wind tunnel tests or real flight tests. Despite its importance, the validation of aerodynamic models based on flight test data for fixed-wing UAVs remains an underdeveloped research area. Therefore, this study aims to analyse the accuracy of aerodynamic coefficients obtained from CFD simulations and to formulate a UAV dynamic model based on CFD aerodynamic data in a systematic way. The model's response is subsequently compared with flight test data to assess the fidelity of the CFD simulation in representing actual flight conditions. Additionally, the study highlights the causes of discrepancies between CFD simulation results and flight test data. Informed by these findings, recommendations are presented to enhance the accuracy of UAV dynamic models in the field of CFD-based aerodynamic modelling.

2 Methodology

2.1 UAV specification

This study operated fixed-wing UAVs with small twin engines, shown in Fig. 1 and the specification of the UAV is given in Table 1. The missions of this UAV include topographic mapping, land surveying, engineering survey, precision agriculture, and other fields.

2.2 Dynamic simulation using CFD

In this paper, unsteady simulation is used to determine dynamic stability derivatives, which are key parameters for modelling aircraft motion dynamics. The aircraft stability

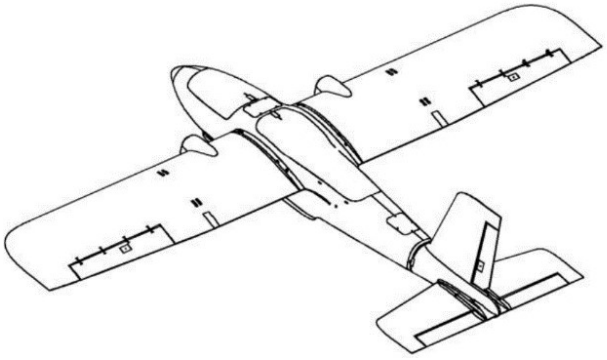

Fig. 1 UAV (makeflyeasy, 2020)

Table 1 The UAV Specification

Parameter	Value	Unit
Material	EPO, EVA, Carbon Fibre, etc.	-
Wingspan	2.43	m
Fuselage Height	1.8	m
Fuselage Length	1.45	m
Wing Area	0.725	m^2
Stall Speed	10	m/s
Wind Resistance	5	m/s
MTOW	11.5	kg
Max Payload	1.5	kg
Practical Lift	6	km
Flight Speed	17-20	m/s

derivatives are obtained through CFD-based transient simulations. The aircraft is simulated by three types of harmonic oscillatory motion models in both the longitudinal and lateral-directional modes. The longitudinal mode includes up-down translation in the z-axis (plunge oscillation), rotation over the y-axis (pitch oscillation), and combined translation-rotation in the z-axis and in the x-axis. Meanwhile the lateral-directional mode includes right-left translation in the y-axis (sway oscillation), rotation over the z-axis (yaw oscillation) and x-axis (roll oscillation), and combined translation-rotation in the y-axis and in the x-axis. The historical data of force and moment coefficients against time from the simulations are processed using Fourier series analysis.

The forces and moments acting on the aircraft in the longitudinal mode can be expressed as a function of the angle of attack, pitch rate, and its time derivative. It can be written in non-dimensional form as defined in Eq. (1),

$$C_i = C_{i_0} + C_{i_\alpha}\alpha + \frac{l_{ref}}{2V}C_{i_{\dot\alpha}}\dot\alpha + \frac{l_{ref}}{2V}C_{i_q}q + \left(\frac{l_{ref}}{2V}\right)^2 C_{i_{\dot q}}\dot q + \ldots , \quad (1)$$

where V denotes the airspeed, $l_{ref} = \bar{c}$ represents the reference length in the longitudinal mode (Mean Aerodynamic Chord) and C_i denotes the non-dimensional aerodynamic coefficient associated with the forces or moments acting on the aircraft in the longitudinal mode. Specifically, C_i represents the lift coefficient (C_L) where $i = L$, drag coefficient (C_D) where $i = D$, and pitching moment coefficient (C_m) where $i = m$. These coefficients quantify the aerodynamic response due to changes in the angle of attack (α), its time derivative $(\dot\alpha)$, pitch rate (q), and its time derivative $(\dot q)$. These coefficients C_i are then used to calculate the aerodynamic forces and moments acting on the aircraft, which are input into the equations of motion to predict the aircraft's dynamic response.

Meanwhile, in the lateral-directional mode, the forces and moments acting on the aircraft are assumed to be a function of the sideslip angle (β), roll rate (p), yaw rate (r), and its time derivative $(\dot\beta, \dot p, \dot r)$. It can be written in non-dimensional form as defined in Eq. (2),

$$C_j = C_{j_0} + C_{j_\beta}\beta + \frac{l_{ref}}{2V}C_{j_{\dot\beta}}\dot\beta + \frac{l_{ref}}{2V}C_{j_p}p + \left(\frac{l_{ref}}{2V}\right)^2 C_{j_{\dot p}}\dot p + \frac{l_{ref}}{2V}C_{j_r}r + \left(\frac{l_{ref}}{2V}\right)^2 C_{j_{\dot r}}\dot r + \ldots \quad (2)$$

where V is the airspeed, $l_{ref} = b$ is the reference length in the lateral-directional mode, which is the wingspan, and C_j denotes the non-dimensional aerodynamic coefficient and are then used to calculate the corresponding aerodynamic forces and moments acting on the aircraft, which are input into the equations of motion to predict the aircraft's dynamic response. Indices $j = Y, l, n$ signify the side force, roll moment, and yaw moment, respectively.

For the forced oscillation approach, the dynamic stability derivatives are obtained by using three simple harmonic oscillation motions; plunging, pitching, and flapping (Mi and Zhan, 2020; Juliawan et al., 2021). To generate these oscillations, each motion requires a unique input combination of translational and rotational velocities along the x-, y-, and z-axis. These inputs are incorporated into the CFD setup through user-defined functions (UDFs) specific to each mode, utilizing the coordinate system wherein the x-axis represents the longitudinal direction and the y- and z-axes represent the lateral-directional plane.

Research of (Juliawan et al., 2021) focused on longitudinal mode, whereas this study investigates both longitudinal and lateral-directional modes. To calculate the dynamic stability derivatives in both modes, the aircraft model is simulated in translational motion, rotational motion, and coupled motions (translational and rotational) in both longitudinal and lateral-directional modes. The simulation of these three harmonic oscillatory motions generates force and moment coefficients over time, which are then approximated using Fourier series to obtain the aircraft stability derivatives.

2.2.1 Translational motion

This motion examines the dynamic stability derivatives by oscillating the aircraft model longitudinally (up and down) and laterally (right and left). Such translational motion minimizes moment coefficients caused by pitch, roll, and

yaw rates. As a result, this motion generates dynamic stability derivatives that are primarily influenced by the angle of attack in the longitudinal mode and by the sideslip angle in the lateral-directional mode. Mathematically, the following equations represent translational motion in the longitudinal and lateral-directional modes.

$$z = z_{\max} \sin\left(k\tau\right) \tag{3}$$

$$y = y_{\max} \sin\left(k\tau\right) \tag{4}$$

The variables z and y represent the aircraft model's position along the z- and y-axes, respectively, relative to the reference frame at a given time. The variables $z_{\max}$ and $y_{\max}$ denote the maximum amplitudes of the forced harmonic oscillations in the longitudinal and lateral-directional modes. The reduced frequency and non-dimensional time are denoted by k and τ, respectively. Figs. 2 and 3 visualize the aircraft's translational motion along the z- and y-axes over a single oscillation period.

During translational motion, induced velocity arises, resulting in a local induced angle of attack (in the longitudinal mode) and a local induced sideslip angle (in the lateral mode).

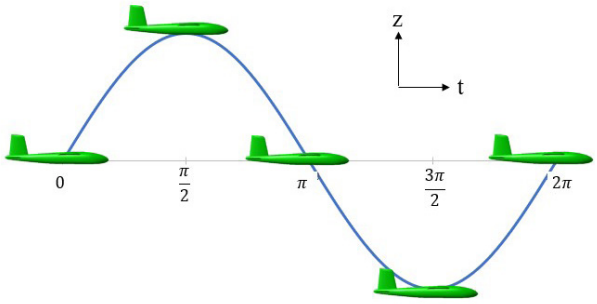

Fig. 2 The aircraft's translational motion along the z-axis over a single oscillation period

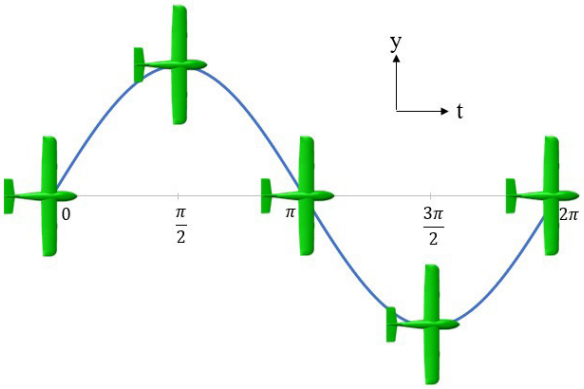

Fig. 3 The aircraft's translational motion along the y-axis over a single oscillation period

Since the motion is harmonic, the induced angle of attack and its rate, as well as the induced angle of sideslip and its rate, can be calculated using the equations below:

$$\alpha = \frac{-\dot{z}}{V_\infty} = \frac{-z_{\max} k \cos\left(k\tau\right)}{V_\infty} = -\alpha_{\max} \cos\left(k\tau\right) \tag{5}$$

$$\dot{\alpha} = \frac{-\ddot{z}}{V_\infty} = \frac{z_{\max} k^2 \sin\left(k\tau\right)}{V_\infty} = \alpha_{\max} k \sin\left(k\tau\right) \tag{6}$$

$$\beta = \frac{-\dot{y}}{V_\infty} = \frac{-y_{\max} k \cos\left(k\tau\right)}{V_\infty} = -\beta_{\max} \cos\left(k\tau\right) \tag{7}$$

$$\dot{\beta} = \frac{-\ddot{y}}{V_\infty} = \frac{z_{\max} k^2 \sin\left(k\tau\right)}{V_\infty} = \beta_{\max} k \sin\left(k\tau\right) \tag{8}$$

where V_∞ denotes the freestream velocity, $\dot{z}$ and $\dot{y}$ denote the time derivative of aircraft model's position along the z- and y-axes and they represent the vertical speed and lateral speed as well. The $\alpha_{\max}$ denotes the maximum angle of attack, and $\beta_{\max}$ denotes the maximum angle of sideslip. Substituting α and $\dot{\alpha}$ into Eq. (1) yields the force and moment coefficients in terms of C_{i_α} and $C_{i_{\dot{\alpha}}}$.

$$C_i\left(k\tau\right) = C_{i_0} - C_{i_\alpha} \alpha_{\max} \cos\left(k\tau\right) + C_{i_{\dot{\alpha}}} \alpha_{\max} k \sin\left(k\tau\right) \tag{9}$$

Eq. (9) is then approximated using a Fourier series as expressed in Eq. (10),

$$C_i\left(k\tau\right) = \frac{a_0}{2} + \sum_{n=1}^{\infty} \left(a_n \cos\left(nk\tau\right) + b_n \sin\left(nk\tau\right)\right) \tag{10}$$

where a_0, a_n, and b_n represent the Fourier series coefficients and indices n represents the Fourier series order.

The approximation yields the values of C_{i_α} and $C_{i_{\dot{\alpha}}}$ by comparing Eqs. (9) and (10). Furthermore, it yields:

$$C_{i_\alpha} = -\frac{a_1}{\alpha_{\max}} \tag{11}$$

$$C_{i_{\dot{\alpha}}} = \frac{b_1}{k\alpha_{\max}} \tag{12}$$

Simulating translational motion in the lateral mode yields stability derivatives C_{j_β} and $C_{j_{\dot{\beta}}}$.

2.2.2 Rotational motion

This motion examines the dynamic stability derivatives by oscillating the aircraft model around its centre of gravity or moment reference point. In the longitudinal mode, the model undergoes pitch rotation, while in the lateral-directional mode, it oscillates through roll and yaw rotations.

This motion produces coupled dynamic stability derivatives, which are influenced by the angle of attack rate and pitch rate in the longitudinal mode and the sideslip angle rate and yaw rate in the directional mode. In this scenario, the local pitch angle corresponds to the local induced angle of attack, while the local yaw angle corresponds to the local induced sideslip angle. The rotational motion in the longitudinal mode can be described mathematically as follows.

$$\theta = \theta_{\max} \cos(k\tau) = \alpha_{\max} \cos(k\tau) \tag{13}$$

$$q = \dot{\theta} = -\theta_{\max} k \sin(k\tau) = -\alpha_{\max} k \sin(k\tau) \tag{14}$$

$$\dot{q} = \ddot{\theta} = -\theta_{\max} k^2 \cos(k\tau) = -\alpha_{\max} k^2 \cos(k\tau) \tag{15}$$

The following equation expresses rotational motion in the directional mode, assuming that the angle of attack is zero.

$$\psi = \psi_{\max} \cos(k\tau) = \beta_{\max} \cos(k\tau) \tag{16}$$

$$r = \dot{\psi} = -\psi_{\max} k \sin(k\tau) = -\beta_{\max} k \sin(k\tau) \tag{17}$$

$$\dot{r} = \ddot{\psi} = -\psi_{\max} k^2 \cos(k\tau) = -\beta_{\max} k^2 \cos(k\tau) \tag{18}$$

Because rotational motion about the x-axis (rolling motion) is not strongly coupled with the beta angle, the rotational motion in the lateral mode can be described as follows, assuming both angle of attack and sideslip angles are zero.

$$\phi = \phi_{\max} \cos(k\tau) \tag{19}$$

$$p = \dot{\phi} = -\phi_{\max} k \sin(k\tau) \tag{20}$$

$$\dot{p} = \ddot{\phi} = -\phi_{\max} k^2 \cos(k\tau) \tag{21}$$

Figs. 4–6 illustrate the aircraft's rotational motion with regard to the y-axis (pitch), x-axis (roll), and z-axis (yaw) over a single oscillation period.

Substituting α, $\dot{\alpha}$, q, and $\dot{q}$ into Eq. (1) yields the following force and moment coefficients:

$$C_i(k\tau) = C_{i_0} + \alpha_{\max}\left(C_{i_\alpha} - k^2 C_{i_{\dot{q}}}\right)\cos(k\tau) - \alpha_{\max} k\left(C_{i_{\dot{\alpha}}} + C_{i_q}\right)\sin(k\tau) \tag{22}$$

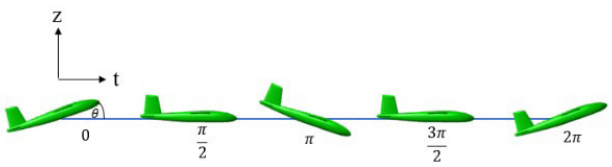

Fig. 4 The aircraft's rotational motion with regard to the y-axis (pitch) over a single oscillation period

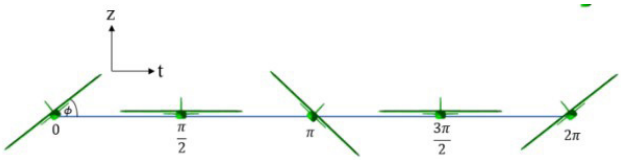

Fig. 5 The aircraft's rotational motion with regard to the x-axis (roll) over a single oscillation period

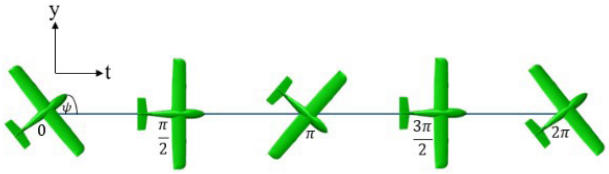

Fig. 6 The aircraft's rotational motion with regard to the z-axis (yaw) over a single oscillation period

Eq. (22) is then approximated using the Fourier series in Eq. (10), yielding the following stability derivatives.

$$C_{i_{\dot{\alpha}}} + C_{i_q} = -\frac{b_1}{k\alpha_{\max}} \tag{23}$$

Substituting β, $\dot{\beta}$, r, and $\dot{r}$ into Eq. (2) yields the following force and moment coefficients in the lateral-directional mode:

$$C_j(k\tau) = C_{j_0} + \beta_{\max}\left(C_{j_\beta} - k^2 C_{j_{\dot{r}}}\right)\cos(k\tau) - \beta_{\max} k\left(C_{j_{\dot{\beta}}} + C_{j_r}\right)\sin(k\tau) \tag{24}$$

Eq. (24) is then approximated using the Fourier series in Eq. (10) in terms of C_j to provide the stability derivatives as shown below.

$$C_{j_{\dot{\beta}}} + C_{j_r} = -\frac{b_1}{k\beta_{\max}} \tag{25}$$

Because rotational motion about the x-axis (rolling motion) has no meaningful correlation with the beta angle, the beta angle and its derivative are assumed to be zero. Substituting p and $\dot{p}$ into Eq. (2) yields the force and moment coefficients for lateral-directional mode:

$$C_j = C_{j_0} - \phi_{\max} k^2 C_{j_{\dot{p}}} \cos(k\tau) - \phi_{\max} k C_{j_p} \sin(k\tau) \tag{26}$$

The equation is then approximated using the Fourier series to yield the stability derivatives shown as follows.

$$C_{j_p} = -\frac{b_1}{k\phi_{\max}} \tag{27}$$

2.2.3 Coupled motion (translation and rotation)

In the longitudinal mode, the aircraft model oscillates translationally along the z-axis while rotating continuously around the y-axis. This motion eliminates any variation in the aircraft's angle of attack relative to the free stream. In the lateral-directional mode, this motion is generated by translating the aircraft model along the y-axis while rotating continuously about the z-axis. This motion, like in the longitudinal mode, prevents any change in the sideslip angle relative to the free stream. Since the angle of attack and sideslip angle remain constant, the pitch rate varies in the longitudinal mode, while the yaw rate varies in the lateral-directional mode. Figs. 7 and 8 illustrate the aircraft's coupled motion in the longitudinal and lateral-directional modes over a single oscillation period.

Substituting q and $\dot{q}$ into Eq. (1) yields the force and moment coefficients:

$$C_i(k\tau) = C_{i_0} - \alpha_{\max} k C_{i_q} \sin(k\tau) - \alpha_{\max} k^2 C_{i_{\dot{q}}} \cos(k\tau) \tag{28}$$

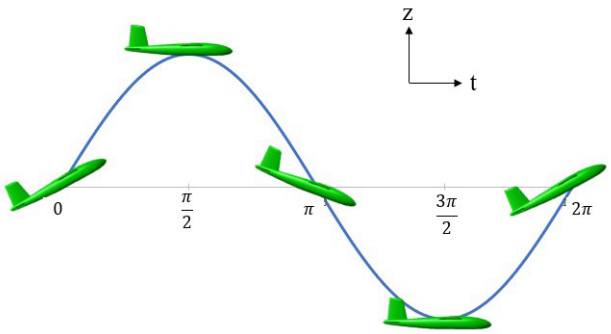

Fig. 7 The aircraft's coupled motion in the longitudinal mode over a single oscillation period

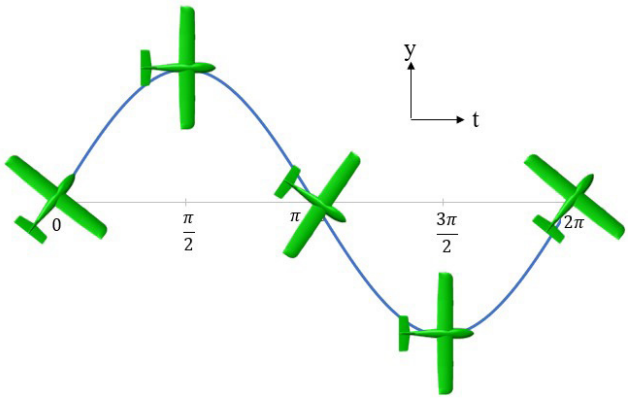

Fig. 8 The aircraft's coupled motion in the lateral-directional mode over a single oscillation period

Eq. (28) is then approximated using the Fourier series in Eq. (10) in terms of C_i to yield the stability derivatives shown below.

$$C_{i_q} = -\frac{b_1}{k\alpha_{\max}} \tag{29}$$

Substituting r and $\dot{r}$ into Eq. (2) yields the force and moment coefficients for the lateral-directional mode:

$$C_j(k\tau) = C_{j_0} - \beta_{\max} k C_{j_r} \sin(k\tau) - \beta_{\max} k^2 C_{j_{\dot{r}}} \cos(k\tau) \tag{30}$$

The equation is then approximated using the Fourier series to yield the stability derivatives shown below.

$$C_{j_r} = -\frac{b_1}{k\beta_{max}} \tag{31}$$

When simulating the aircraft's oscillatory motion, reduced frequency becomes a key parameter, representing both the frequency of oscillation as well as the degree of flow unsteadiness. Table 2 summarizes the relationship between flow unsteadiness and reduced frequency (Leishman, 2006; Moelyadi et al., 2019). Reduced frequency is a dimensionless parameter, and its value can be calculated using Eq. (32),

$$k = \frac{\omega l}{V_\infty} = \frac{2\pi f l}{V_\infty}, \tag{32}$$

where k is the reduced frequency, ω is the angular velocity, f is the frequency of oscillation, and V_∞ is the freestream velocity.

2.3 Mathematical model

Modelling aircraft motion is essential for designing an aircraft's control system. Additionally, the formulation of the aircraft's equations of motion commonly known as six degrees of freedom (6 DOF) is crucial for the research and development of software-in-the-loop simulations and hardware-in-the-loop simulations. With this modelling, an evaluation of aircraft stability can be obtained.

Table 2 The relationship between flow unsteadiness and reduced frequency

Degree of unsteadiness	The value of reduced frequency
Steady	$k = 0$
Quasi-steady	$0 < k < 0.05$
Unsteady	$0.05 < k < 0.2$
Highly unsteady	$0.2 > k$

Aircraft motion modelling generally consists of three components: the aerodynamic model, which includes aerodynamic forces and moments; the weight model; and the thrust model. The equations of motion are represented by block diagrams in Simulink, hereinafter called as the dynamic model.

The equations of motion developed in this paper include both the longitudinal and lateral-directional equations of motion. The longitudinal equations govern the aircraft's motion in the vertical plane, encompassing changes in pitch angle, altitude, and forward velocity. These equations incorporate aerodynamic forces such as lift and drag, along with propulsion and gravitational forces acting along the aircraft's longitudinal axis.

Meanwhile, the lateral-directional equations describe the aircraft's motion in the horizontal plane, including roll, yaw, and side-slip behaviour. These equations determine the aircraft's response to lateral aerodynamic forces and moments, which are primarily influenced by control surfaces such as the ailerons and rudder, as well as by asymmetric thrust.

2.3.1 Aerodynamic model

The longitudinal and lateral-directional aerodynamic models play a crucial role in understanding and predicting an aircraft's stability and control characteristics. These models are developed using various approaches and are essential during both the design and operational phases. A key aspect of these models is the estimation of aerodynamic derivatives, which quantify how aerodynamic forces and moments vary with changes in flight conditions. In this study, Computational Fluid Dynamics (CFD) is employed to estimate these derivatives, providing a high-fidelity numerical approach that complements wind tunnel testing and flight data.

Simulations using Computational Fluid Dynamics (CFD) include both steady and unsteady approaches. Steady simulations assume constant flow properties over time and are used for equilibrium conditions, such as cruise flight, requiring less computational effort. In contrast, unsteady simulations capture time-dependent flow variations and are essential for analysing transient aerodynamic phenomena, such as gust responses, vortex shedding, and dynamic stability. These simulations are crucial for studying aircraft manoeuvres and other dynamic flight conditions.

Aerodynamics Model in Longitudinal:

$$F_{Lift} = \frac{1}{2}\rho V^2 S\left[C_{L_0} + C_{L_\alpha}\alpha + C_{L_q}\frac{\bar{c}}{2V}q + C_{L_{\delta_e}}\delta_e\right] \tag{33}$$

$$F_{Drag} = \frac{1}{2}\rho V^2 S\left[C_{D_0} + C_{D_\alpha}\alpha + C_{D_q}\frac{\bar{c}}{2V}q + C_{D_{\delta_e}}\delta_e\right] \tag{34}$$

$$m = \frac{1}{2}\rho V^2 S\,\bar{c}\left[C_{m_0} + C_{m_\alpha}\alpha + C_{m_q}\frac{\bar{c}}{2V}q + C_{m_{\delta_e}}\delta_e\right] \tag{35}$$

Aerodynamic Model in Lateral-Directional:

$$F_{side} = \frac{1}{2}\rho V^2 S\begin{bmatrix} C_{Y_0} + C_{Y_\beta}\beta + C_{Y_r}\frac{b}{2V}r \\ +C_{Y_p}\frac{b}{2V}p + C_{Y_{\delta_a}}\delta_a + C_{Y_{\delta_r}}\delta_r \end{bmatrix} \tag{36}$$

$$l = \frac{1}{2}\rho V^2 Sb\begin{bmatrix} C_{l_0} + C_{l_\beta}\beta + C_{l_r}\frac{b}{2V}r \\ +C_{l_p}\frac{b}{2V}p + C_{l_{\delta_a}}\delta_a + C_{l_{\delta_r}}\delta_r \end{bmatrix} \tag{37}$$

$$n = \frac{1}{2}\rho V^2 Sb\begin{bmatrix} C_{n_0} + C_{n_\beta}\beta + C_{n_r}\frac{b}{2V}r \\ +C_{n_p}\frac{b}{2V}p + C_{n_{\delta_a}}\delta_a + C_{n_{\delta_r}}\delta_r \end{bmatrix} \tag{38}$$

where F_{Lift}, F_{Drag}, and F_{side} denote the lift, drag, and side force, respectively, while l, m, and n represent the pitching, rolling, and yawing moments. The variables V and S are the airspeed and wing reference area, respectively. The coefficients C_L, C_D, and C_Y represent the aerodynamic force coefficients for lift, drag, and side force. The coefficients C_m, C_l, and C_n represent the aerodynamic moment coefficients for pitch, roll, and yaw. The terms α and β are the angle of attack and angle of sideslip, while q, p, and r are the pitch, roll, and yaw rates. The variables δ_e, δ_a, and δ_r are the elevator, aileron, and rudder deflections, respectively. The parameters $\bar{c}$ and b denote the mean aerodynamic chord and wingspan.

In this paper, steady simulations are conducted to obtain dynamic stability derivatives resulting from control surface deflections, including aileron, rudder, and elevator movements. Meanwhile, unsteady simulations are performed to determine stability derivatives induced by variations in pitch rate, roll rate, yaw rate, angle of attack rate, and sideslip angle rate.

To obtain these dynamic stability derivatives, CFD simulations are carried out by applying translational motion, rotational motion, and a combination of both along each coordinate axis. The resulting data are then incorporated into the aerodynamic model as follows.

2.3.2 Weight model

The weight force acting on the aircraft can be resolved into components acting in each of the three axes of the aircraft. When the aircraft is disturbed, these components vary according to the perturbations in attitude thereby contributing to the disturbed motion. Thus, the gravitational contribution is obtained by resolving the aircraft weight into the disturbed body axes (Cook, 2007). The aircraft weight can be determined by multiplying the acceleration due to the gravity by the total mass of the aircraft, as expressed in Eq. (39) (Mulder, 2011).

$$W = mg \tag{39}$$

Eq. (40) expresses the component of weight force in the aircraft body axes.

$$F_G = \begin{bmatrix} F_{G_x} \\ F_{G_y} \\ F_{G_z} \end{bmatrix}_b = \begin{bmatrix} -W\sin\theta \\ W\sin\phi\cos\theta \\ W\cos\phi\cos\theta \end{bmatrix} \tag{40}$$

Since the origin of the aircraft body axes coincides with the centre of gravity (c.g), the weight force acts at the c.g.

Consequently, there is no weight moment about any of the axes, as represented in Eq. (41).

$$L_G = M_G = N_G = 0 \tag{41}$$

2.3.3 Thrust model

The throttle lever angle directly governs the engine power output and, consequently, the generated thrust. Adjusting the throttle lever modifies the thrust magnitude, which subsequently affects the aerodynamic forces and moments acting on the aircraft (Cook, 2007). The thrust force in the body-fixed coordinate system is represented as a vector, as defined in Eq. (42),

$$F_T = \begin{bmatrix} F_{T_x} \\ F_{T_y} \\ F_{T_z} \end{bmatrix}_b = \begin{bmatrix} T\cos\phi_T \\ 0 \\ -T\sin\phi_T \end{bmatrix}, \tag{42}$$

where ϕ_T represents the angle between the body-axis x-direction and the thrust vector. The thrust magnitude is determined using Eq. (43), while the motor torque is computed according to Eq. (44) (Kamal et al., 2015).

$$T = C_T \rho n^2 D^4 \tag{43}$$

$$Q = C_q \rho n^2 D^5 \tag{44}$$

The variable T denotes the thrust magnitude and Q denotes the motor torque. C_T and C_q are the non-dimensional thrust and torque coefficients, respectively. The variable n is the propeller rotation speed in revolutions per second (RPS), and D is the propeller diameter in meter. The propulsion moment in the body axes is expressed in Eq. (45),

$$M_T = \begin{bmatrix} L_T \\ M_T \\ N_T \end{bmatrix}_b = \begin{bmatrix} 0 \\ r_T T \\ 0 \end{bmatrix}, \tag{45}$$

where r_T represents the distance between the thrust and the c.g. of the aircraft. (Yechout et al., 2003; Luckner, 2007; Bahri, 2018).

2.4 Flight test procedure

In this research, three flight tests were undertaken approximately at an altitude of 300 meters and a speed of 17-20 m/s. All three flights were conducted in manual mode. This was done to assess the aircraft's natural response characteristics following input commands. Therefore, there is no difference in the mode or procedure among the three flight tests.

The input deflections applied were elevator singlet, elevator doublet, aileron singlet, aileron doublet, rudder singlet, and rudder doublet, in order to excite the natural response of the UAV.

Before the flight test, the aircraft's condition was inspected, including its weight, centre of gravity, battery, servos, control surfaces, and wind conditions, as shown in Fig. 9. The aircraft weighed approximately 7.5 kg, with a c.g in the x-direction located at about 0.25 of the Mean Aerodynamic Chord (MAC).

During the first flight, wind speed was 5.3 m/s from the northwest, and the weather was cloudy and windy. For the

Fig. 9 Checklist before flight test

subsequent flight test, wind speed was 0.5 m/s under clear weather conditions. On the final flight, wind speed remained at 0.5 m/s

The following is a detailed procedure of the flight tests conducted on UAVs in both longitudinal and lateral/directional modes. The procedure is presented in Table 3 for the trim condition, Table 4 for the longitudinal mode, and Tables 5 and 6 for the lateral/directional mode.

Table 3 Trim condition

No.	Task	Time (sec)
1	Put the aircraft in a stable cruising condition to ensure trim	5
2	Let the aircraft fly freely: 2.1. Check to ensure that the aircraft speed changes within ±0.5 m/s (±1 knot) and the height is ±6 m (±20 ft) 2.2. Record and save the control settings at this trim condition.	5
	Total execution time	10

Table 4 Longitudinal mode procedure

No.	Task	Time (sec)
1	Trim the aircraft for the first short-period mode test	10
2	Provide singlet elevator input	2
3	Let the aircraft fly freely	20
4	Return to the 'race track' pattern so that the aircraft does not leave the controllable visual range	30
5	Trim the aircraft for the second short-period mode test	10
6	Provide doublet elevator input	3
7	Let the aircraft fly freely for	20
8	Return to the 'race track' pattern so that the aircraft does not leave the controllable visual range	30
	Total execution time	125

Table 5 Lateral/directional mode procedure (roll subsidence)

No.	Task	Time (sec)
1	Trim the aircraft for the first roll-subsidence mode test	10
2	Provide singlet aileron input	2
3	Let the aircraft fly freely	20
4	Return to the 'race track' pattern so that the aircraft does not leave the controllable visual range	30
5	Trim the aircraft for the second roll-subsidence mode test	10
6	Provide doublet aileron input	3
7	Let the aircraft fly freely	20
8	Return to the 'race track' pattern so that the aircraft does not leave the controllable visual range	30
	Total execution time	125

Table 6 Lateral/directional mode procedure (spiral and Dutch roll)

No.	Task	Time (sec)
1	Trim the aircraft for the Spiral mode test	10
2	Provide singlet rudder input	2
3	Let the aircraft fly freely	20
4	Return to the 'race track' pattern so that the aircraft does not leave the controllable visual range	30
5	Trim the aircraft for the Dutch roll mode test	10
6	Provide doublet rudder input	3
7	Let the aircraft fly freely	20
8	Return to the 'race track' pattern so that the aircraft does not leave the controllable visual range	30
	Total execution time	125

When the aircraft reaches cruise condition, it is first switched from auto to manual mode and then held in a trimmed state for approximately 10 seconds, as shown in Fig. 10. The pilot then provides inputs to the elevator, aileron, or rudder.

The UAV is allowed to fly freely to observe its dynamic characteristics. During this phase, flight test engineers on the ground monitor the data, as illustrated in Fig. 11. After approximately 10–20 seconds, the pilot regains control, and the system is switched back to auto mode.

3 Result and discussion

3.1 Flight test result

Flight tests for each input were conducted three times across three different days. This approach was adopted for several reasons: to capture the system's response to various inputs, to validate system consistency, and to minimize the influence of noise and external disturbances. The selection of test days from February to August was based on favourable weather forecasts and the availability of required tools and materials.

Fig. 10 The UAV flying in the air

Fig. 11 Pilot observing the UAV, providing input and logging data

UAV systems can exhibit different responses depending on the type of control input applied (elevator, aileron, or rudder). In this study, both singlet and doublet inputs were applied for each control mode. By applying a variety of input types, the aim was to capture a more comprehensive representation of the UAV's dynamic behaviour.

Repeated tests with different inputs also ensure that the UAV system behaves consistently and is not affected by adverse external conditions. In addition, this approach helps to distinguish the actual system response from noise or temporary effects.

In general, the three datasets show consistent trends across elevator, aileron and rudder inputs, whether singlet or doublet. This section presents a comparison of the three datasets in the longitudinal mode, represented by the singlet elevator input, shown in Fig. 12 and in the lateral/directional mode, represented by the singlet rudder input, shown in Fig. 13. Some yaw angle measurements from the flight test exhibited large discrepancies due to different initial values. Specifically, during the singlet rudder inputs on 18 and 19 February, the aircraft exhibited large yaw angles, indicating significant turning, whereas on 5 August, the yaw angle values were notably smaller.

There are very sharp changes in this data due to the angle wrap-around effect, because yaw is a periodic angle (0° = 360°, or 0 rad = 2π rad). Navigation systems or flight data recorders usually store angles within the range [−π, π] or [0, 2π]. This can create the appearance of sudden discontinuities, even though the aircraft may have been continuously turning clockwise or counterclockwise.

The singlet rudder inputs excite the spiral modes; it can be seen from the figure that the roll and yaw values remain stable. Therefore, based on the observed responses, the aircraft can be considered stable in these modes.

3.2 Simulations results from dynamic model and comparison with flight test data

In this section, the aerodynamic coefficients simulated using CFD are shown in Table 7 where they are included in the UAV dynamic model with units of per radian (/rad).

The coefficients are then put into the dynamic model in Simulink as the aerodynamic model to further observe the resulting response. In the dynamic model, the inputs given are the same as those used during the flight test. The simulation time and time step are also matched to the flight test conditions. In the longitudinal mode, the elevator inputs

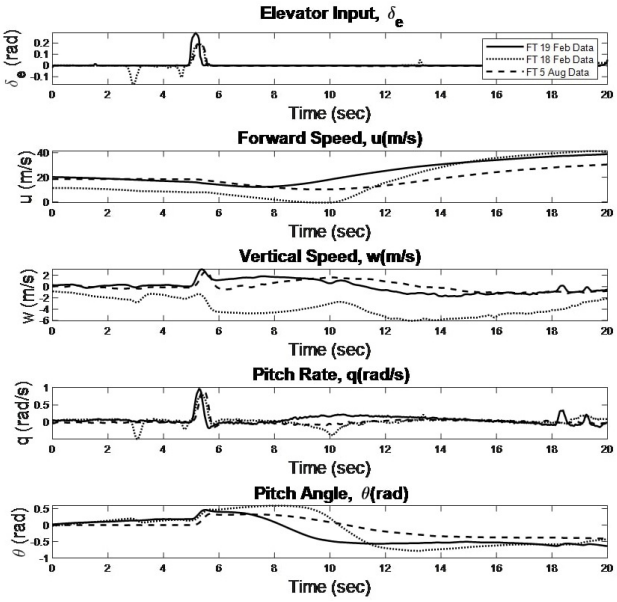

Fig. 12 The result of flight test using elevator input: singlet

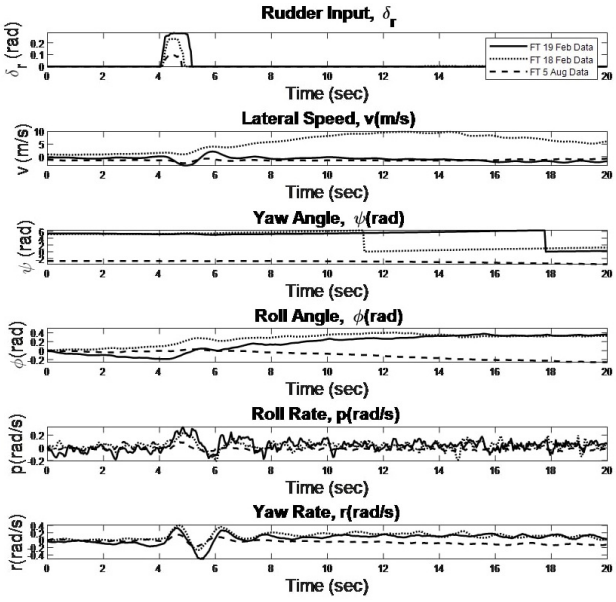

Fig. 13 The result of flight test using rudder input: singlet

Table 7 List of aerodynamics parameter

Parameter	Meaning	Value
C_{D_0}	The coefficient of drag where other variables are zero	0.0244
C_{D_α}	The coefficient of drag due to angle of attack	−0.2658
C_{D_q}	The coefficient of drag due to pitch motion	−0.1739
$C_{D_{\delta_e}}$	The coefficient of drag due to elevator deflection	0.0280
C_{L_0}	The coefficient of lift where other variables are zero	0.4328
C_{L_α}	The coefficient of lift due to angle of attack	4.4582
$C_{L_{\dot{\alpha}}}$	The coefficient of lift due to angle of attack rate	−3.0984
C_{L_q}	The coefficient of lift due to pitch rate	9.3498
$C_{L_{\delta_e}}$	The coefficient of lift due to elevator deflection	0.2922
C_{m_0}	The coefficient of pitching moment where other variables are zero	−0.0073
C_{m_α}	The coefficient of pitching moment due to angle of attack	−0.7993
$C_{m_{\dot{\alpha}}}$	The coefficient of pitching moment due to angle of attack rate	−3.2484
C_{m_q}	The coefficient of pitching moment due to pitch rate	−9.4469
$C_{m_{\delta_e}}$	The coefficient of pitch moment due to elevator deflection	−0.7270
C_{Y_0}	The coefficient of side force where other variables are zero	0
C_{Y_β}	The coefficient of side force due to sideslip angle	−0.2968
$C_{Y_{\dot{\beta}}}$	The coefficient of side force due to sideslip angle rate	−0.0875
C_{Y_p}	The coefficient of side force due to roll rate	−0.0354
C_{Y_r}	The coefficient of side force due to yaw rate	0.3010
$C_{Y_{\delta_a}}$	The coefficient side force due to aileron deflection	0.0057
$C_{Y_{\delta_r}}$	The coefficient side force due to rudder deflection	0.0917
C_{l_β}	The coefficient of roll moment due to sideslip angle	−0.0598
$C_{l_{\dot{\beta}}}$	The coefficient of roll moment due to sideslip angle rate	1.1978
C_{l_p}	The coefficient of roll moment due to roll rate	−0.7660
C_{l_r}	The coefficient of roll moment due to yaw rate	1.0548
$C_{l_{\delta_a}}$	The coefficient of rolling moment due to ailerons deflections	0.1432
$C_{l_{\delta_r}}$	The coefficient roll moment due to rudder deflection	−0.0040
C_{n_β}	The coefficient of yaw moment due to sideslip angle	0.0582
$C_{n_{\dot{\beta}}}$	The coefficient of yaw moment due to sideslip angle rate	−0.0926
C_{n_p}	The coefficient of yaw moment due to roll rate	−0.1249
$C_{n_{\dot{p}}}$	The coefficient of yaw moment due to roll acceleration	0
C_{n_r}	The coefficient of yaw moment due to yaw rate	−0.0258
$C_{n_{\delta_a}}$	The coefficient of yawing moment due to ailerons deflections	−0.0057
$C_{n_{\delta_r}}$	The coefficient yaw moment due to rudder deflection	0.0286

are given singlet and doublet, while for the lateral/directional mode, the aileron and rudder inputs are given singlet and doublet. This was done to avoid overfitting to a singlet type of input and to support validation and verification of the dynamic model.

Using only one type of input may cause the model to lack generality and accuracy when tested with other inputs. Furthermore, since the UAV dynamic model serves as the basis for the control system, simulating with various inputs is important to verify whether the model is able to accurately represent the UAV's actual response across different input scenarios. Finally, the simulation results will be directly compared with flight test data. The flight test data used for input and comparison are outlined in Table 8.

In general, for both modes, the simulation data and flight test data have similar trends. The main differences lie in the magnitude of the responses, and in some parameters, the simulation results oscillate more than the flight test data. This may be because the simulation is more responsive to the inputs and is based on an idealized environment. In this model and flight test data, a positive elevator input indicates nose-up or pitch-up. So, the response in Figs. 14 and 15 correctly reflect the expected behaviour following the input. Singlet input elevators are typically used for phugoid mode excitation and are usually held for several seconds. However, due to limitations, the singlet input given only lasts about one second. According to M.V Cook in his book Flight Dynamic, the phugoid mode is a lightly damped, low-frequency oscillation in forward velocity (u) that is coupled with the pitch angle and altitude (Cook, 2007).

Fig. 14 indicates that the forward speed and pitch angle experience a change or spike from their trim position, followed by slow oscillations, clearly indicating the presence of the phugoid mode. The vertical speed and pitch rate also exhibit sharp spikes but stabilize relatively quickly. Between the 18th and 20th seconds, small disturbances are observed, which may be due to pilot input, hardware interference, or environmental factors during the flight.

Until to the 20th second, the forward speed and pitch angle continue to oscillate, indicating that the phugoid mode has not yet stabilized. Since the simulation was only run up to 20 seconds, it remains unclear when the oscillations would eventually damp out.

Furthermore, to excite the short-period mode, a doublet input is given (Kamal et al., 2016). The short-period mode is usually a damped oscillation in pitch around the y-axis. Whenever the aircraft is disturbed from its pitch equilibrium state, this mode is excited and appears as a classical second-order oscillation, where the main variables are incidence, pitch rate, and pitch angle (Cook, 2007). Whereas according to Kamal et al., the short period mode

Table 8 List of trim condition each of input

No.	Input	H (m)	V (m/s)
1	Elevator Singlet	310	15
2	Elevator Doublet	302	19
3	Aileron Singlet	285	18
4	Aileron Doublet	302	18
5	Rudder Singlet	293	17
6	Rudder Doublet	284	17

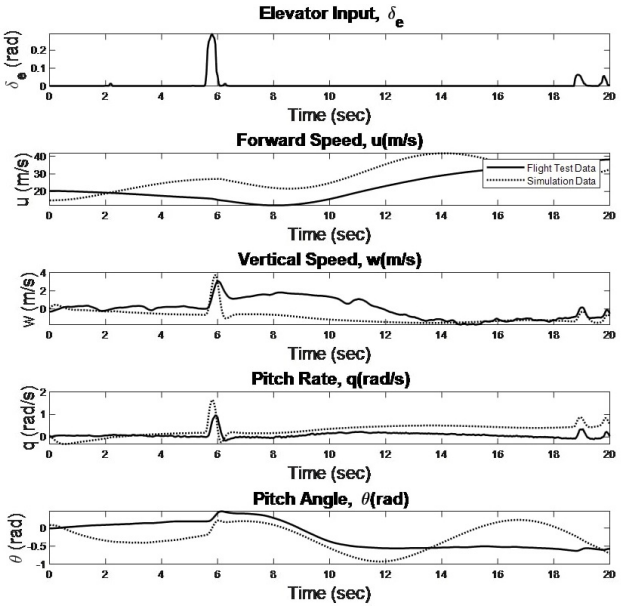

Fig. 14 The result of dynamic model simulation and flight test using elevator input: singlet

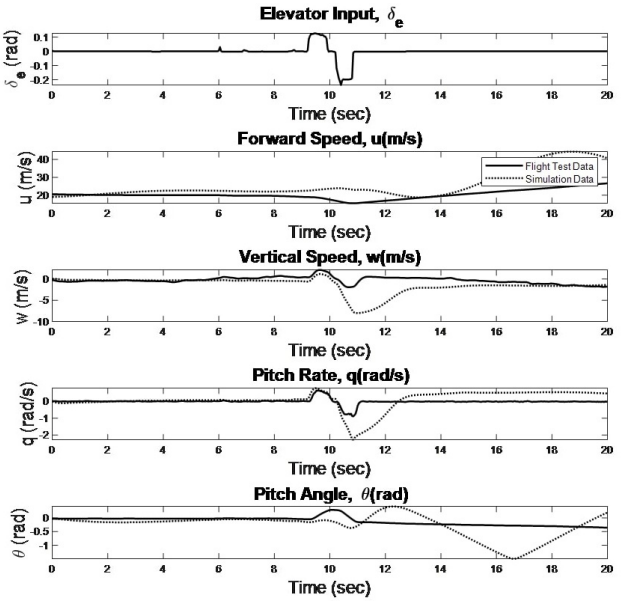

Fig. 15 The result of dynamic model simulation and flight test using elevator input: doublet

is characterized by variation of angle of attack and pitch rate, while the forward velocity remains nearly constant (Kamal et al., 2016). As shown in Fig. 15, the pitch rate is quickly damped. In contrast, the pitch angle shows slower oscillations. Based on these observations, the short-period mode has stabilised, as shown in Fig. 15.

It should be noted that the forward speed from flight test data also increases, as seen in Figs. 14 and 15. However, the simulated data shows more oscillation. When a singlet input is applied, the vertical speed changes and then stabilizes. However, the values from the flight test are higher than those from the simulation, as seen in Fig. 14.

Pitch rate values in simulation and flight test data are very similar for Fig. 14, while in Fig. 15 there is still a considerable difference after the input is applied. Regarding the pitch angle, when either singlet or doublet elevator inputs are given, the simulation data continues to oscillate, while the flight test data is more stable. It may be worthwhile to re-examine certain aerodynamic coefficients related to pitch dynamics, such as C_{m_q}, C_{m_α} and $C_{m_{\dot{\alpha}}}$. C_{m_α} has a great influence on the static stability and response of the system to the angle of attack. $C_{m_{\dot{\alpha}}}$ has an influence on the dynamic stability and response of the system to changes in angle of attack. C_{m_q} has an influence on the dynamic stability and response of the system to pitch rate. In terms of forward speed, the model currently does not include the CDu coefficient. Adding this coefficient in future iterations may help reduce the oscillations in forward speed and allow it to stabilize more quickly.

When an aileron input is applied, the model response and flight test data produce the expected results, as shown in Figs. 16 and 17. A singlet aileron input can be used to excite the roll subsidence mode (Kamalet al., 2016). This mode is typically excited by applying a short-duration square pulse to the ailerons, while the other control surfaces remain fixed at their trim settings. The simulation results in Fig. 16 show that the lateral speed, roll angle, yaw rate, and roll rate exhibit oscillatory behaviour.

The simulation results in Fig. 17 show that oscillations are most pronounced in the roll angle, followed by lateral speed and yaw rate, while the roll rate appears to be the most stable. The clearest indication of the roll subsidence mode is observed in the roll rate response, which stabilizes faster than both the yaw rate and lateral speed. A similar trend is seen in the lateral speed, which also stabilizes more quickly than the roll angle. The roll angle, however, tends to oscillate more slowly. As for the yaw angle, the aircraft can be seen turning and then returning to its original heading around the 19th second.

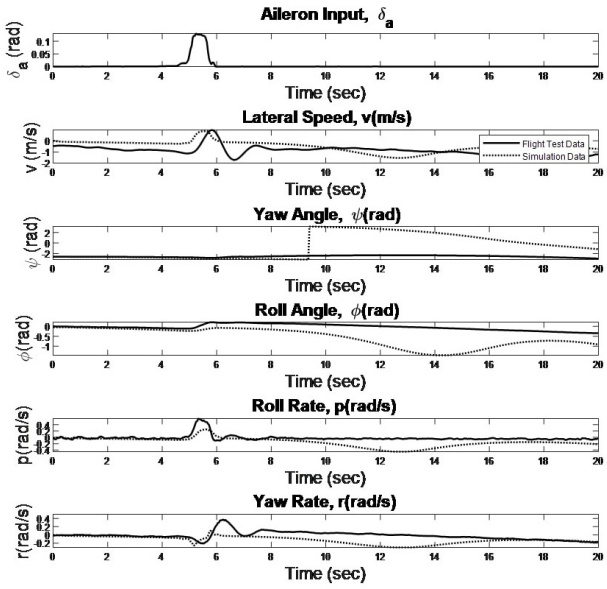

Fig. 16 The result of dynamic model simulation and flight test using aileron input: singlet

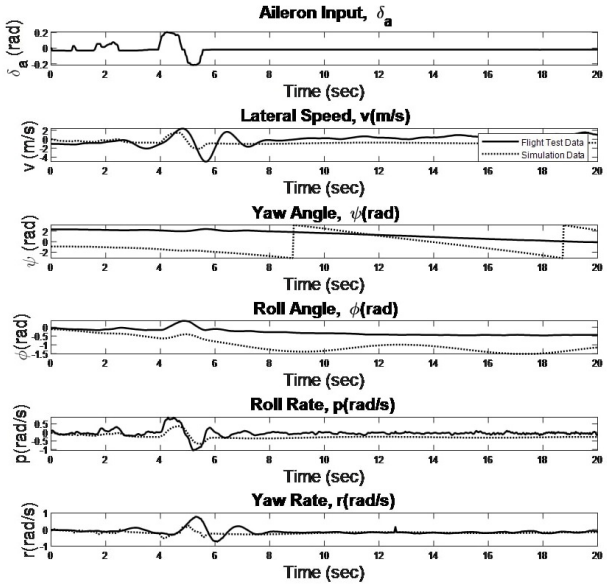

Fig. 17 The result of dynamic model simulation and flight test using aileron input: doublet

It can be seen from Fig. 16 that there is a difference in yaw angle between flight test and simulation results. Both data indicate that the aircraft is turning. However, the flight test data appears smoother, while the simulation results seem to have discontinuities. As mentioned in the previous section, this may be due to the angle wrap-around effect, which can also occur in simulations. The other parameters show a generally similar trend. Then, when the aileron is given doublet input, as shown in Fig. 17, the differences between the simulation and flight test data become more significant—particularly in the roll angle and yaw angle

response. Singlet rudder inputs can be used to excite spiral modes. When triggered, these modes typically develop slowly and involve complex, coupled motions in roll, yaw, and sideslip. It can be seen in Fig. 18 that when the aircraft is given a singlet rudder input, the aircraft begins to turn around the 12th second, after which the yaw angle stabilizes at a certain value (observed in yaw angle). The roll angle increases in response to the input, decreases around the 12th second, and then begins to rise again. Both roll and yaw rates also show changes when input is given input and then begin to stabilize around the same time

Furthermore, the rudder doublet input is used to excite the Dutch roll mode. The Dutch roll mode is a classical damped oscillation in yaw, around the z-axis of the aircraft, which is coupled with roll and, to a lesser extent, sideslip. The aircraft's lateral speed changes when the input is given and then appears more stable around the 14th second. The yaw angle begins to change shortly after the input is applied between the 7th and 9th seconds, with the aircraft starting to turn around the 8th second. Similarly, the roll angle starts to increase following the input and then decreases and increases again until the 20th second, showing slow oscillations. The roll and yaw rates also respond to the input and begin to stabilize around the 14th second.

When singlet and doublet rudder inputs are given to the aircraft, the flight test results are more ripple than the simulation results, particularly in terms of the yaw rate and roll rate. The most noticeable ripple is in the roll rate of the flight test results. As shown in Figs. 18 and 19, the lateral

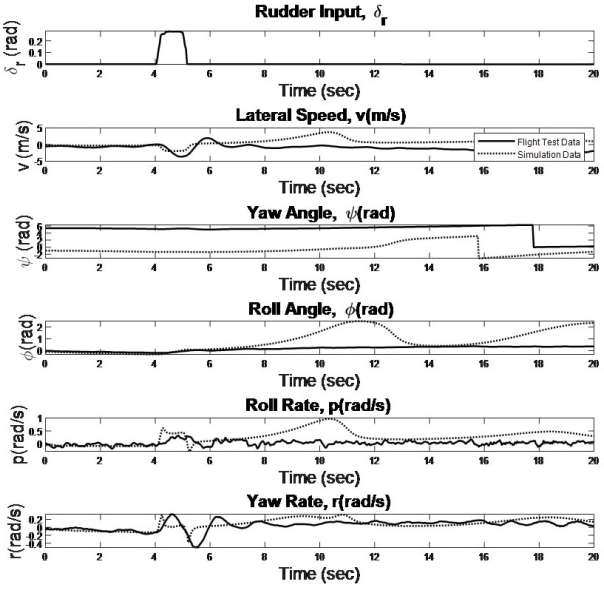

Fig. 18 The result of dynamic model simulation and flight test using rudder input: singlet

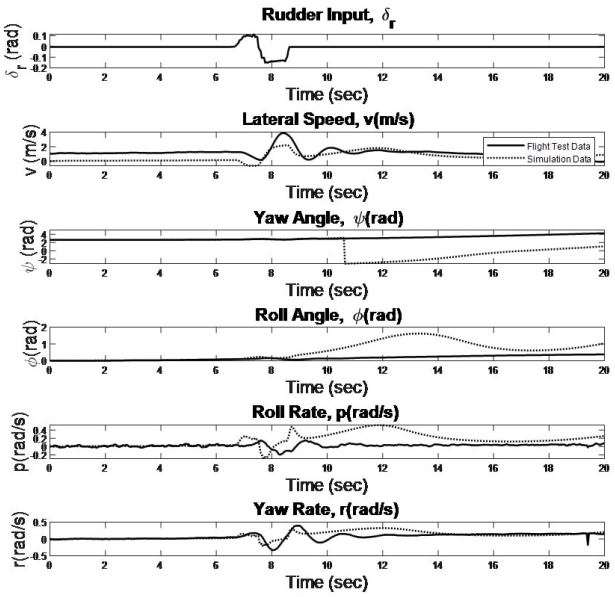

Fig. 19 The result of dynamic model simulation and flight test using rudder input: doublet

speed trend is almost similar for both input types. For the yaw angle with singlet rudder input, the simulation shows the aircraft turning earlier than in the flight test, possibly because the simulation is more responsive, whereas the flight test may experience some delay. With doublet input, the aircraft begins turning at almost the same time in both the simulation and flight test, although the simulation results display discontinuities. Both responses eventually stabilize. Regarding the roll angle, the simulation results tend to oscillate more than the flight test data.

In addition to visual observation, the Mean Absolute Error (MAE) was calculated. MAE measures the average absolute difference between the simulation results and the flight test data. This metric is more robust to outliers and provides an indication of how far, on average, the predictions deviate from the actual measurements.

$$MAE = \frac{1}{n}\sum_{i=1}^{n}\left|y_{sim,i} - y_{flight,i}\right| \tag{46}$$

Table 9 shows that during the longitudinal mode, the pitch rate and pitch angle values are, on average, closer between the flight test and simulation results compared to the forward speed and vertical speed values. This indicates that the model performs well in capturing the pitching response. The longitudinal model captures the pitch dynamics well (short period and phugoid modes), but is less accurate in modelling translational velocity. This discrepancy may be due to differences in the initial forward speed values between the simulation and flight test. As for the

Table 9 Comparison of MAE values of simulation and flight test results

Input	Parameter	Value
Elevator Singlet	u	7.971
	w	0.9516
	q	0.2828
	θ	0.3457
Elevator Doublet	u	5.5881
	w	1.2902
	q	0.3313
	θ	0.2885
Aileron Singlet	v	0.5702
	ψ	2.1171
	ϕ	0.5195
	p	0.1391
	r	0.1145
Aileron Doublet	v	1.2146
	ψ	2.4903
	ϕ	0.7069
	p	0.2386
	r	0.1002
Rudder Singlet	v	1.9386
	ψ	5.5432
	ϕ	0.6737
	p	0.2582
	r	0.0992
Rudder Doublet	v	0.6916
	ψ	2.159
	ϕ	0.3998
	p	0.1479
	r	0.0685

lateral/directional mode, the yaw rate values in all forms of input excitation, both aileron and rudder, show the closest agreement between flight test results and simulations.

The lateral model is generally good overall, especially for the yaw rate response to doublet rudder inputs. However, the accumulated heading error needs further attention. Similarly, the yaw angle shows differences in its range of values.

4 Conclusion

CFD simulations were successfully conducted to generate the aerodynamic model integrated into the UAV dynamic model. The UAV dynamic model in the form of a 6-DOF model has also been fully developed. This model includes aerodynamic, weight and thrust models.

Flight test data has also been collected during three separate times as part of the validation process. The results showed that each of the flight test data produced response trends that were consistent with the simulations, thus supporting the validity of the model.

Furthermore, the flight test data were compared with the dynamic model response. Overall, the simulation results show the same trend as the flight test data. The response produced expected graphs consistent with the inputs for both longitudinal and lateral/directional modes, as supported by relevant literature and research.

In the longitudinal mode, the singlet elevator input successfully excited the phugoid mode and the doublet elevator input generated the short period mode. However, during the 20 seconds simulation, the pitch angle and forward speed responses still showed oscillations indicating need to reassess the aerodynamic coefficients associated with pitch and the addition of CDu coefficients to the model.

Despite the oscillations, comparison with flight test data shows that the MAE (Mean Absolute Error) values for the pitch rate and pitch angle parameters are the smallest compared to other parameters. This indicates that the response patterns of pitch rate and pitch angle in the simulation have good trend and amplitude agreement, although there are differences in the damping characteristics and final stability. In contrast, the largest MAE value is found in the forward speed parameter, due to the difference in initial values between simulation and flight test data.

In the lateral/directional mode, aileron input successfully generates roll subsidence mode, singlet rudder input generates spiral mode, and doublet rudder input generates Dutch roll mode. Among the lateral parameters, the yaw rate showed the best agreement with the flight test data, while the yaw angle had the largest MAE value due to the difference in angle range between the simulated and actual data.

These findings indicate that CFD-based aerodynamic models validated with flight test data can reliably represent UAV flight dynamics. However, some discrepancies between simulation and flight test data still occur, which are caused by factors such as the inaccuracy of certain aerodynamic coefficients, simplifying assumptions in CFD simulation, and variations in environmental conditions during flight tests.

Future research will focus on parameter identification using flight test data, which will be compared with simulation results, particularly with regard to dynamic characteristics such as eigenvalues and damping ratios. Additionally, subsequent flight tests will be conducted in environments with more stable conditions, as the previous tests took place in a coastal area prone to strong winds, necessitating careful scheduling to minimize weather-induced disturbances.

Acknowledgement

The authors would like to thank the Head of the Research Center for Aeronautics Technology, the Research Group Leader, and the flight test team at the National Research and Innovation Agency (BRIN), Indonesia.

References

Aljuhaishi, S., Al-Timimi, Y. K., Wahab, B. I. (2024) "Comparing Turbulence Models for CFD Simulation of UAV Flight in a Wind Tunnel Experiments", Periodica Polytechnica Transportation Engineering, 52(3), pp. 301–309. https://doi.org/10.3311/pptr.24004

Bahri, S. (2018) "Development of Flight Control Laws for The Basic Electronic Flight Control Systems of The LSA-02 Technology Demonstrator Aircraft", Institut Teknologi Bandung.

Benyamen, H., Chowdhury, M., Keshmiri, S. (2024) "Data-Driven Aircraft Modeling for Robust Reinforcement Learning Control Synthesis With Flight Test Validation", Journal of Dynamic Systems, Measurement, and Control, 146(6), 061105. https://doi.org/10.1115/1.4065804

Consentino, G. B. (2007) "CFD to Flight: Some Recent Success Stories of X-plane Design to Flight Test at the NASA Dryden Flight Research Center", In: 2007 ITEA Symposium, Kaua, HI, USA, pp. 1–9.

Cook, M. V. (2007) "Flight Dynamics Principles", Butterworth-Heinemann. ISBN 978-0-7506-6927-6 https://doi.org/10.1016/b978-0-7506-6927-6.x5000-4

Elbedewy, A. A., Mohamed, S. S., Hamed, H. O. (2021) "Modeling and Simulation of Small UAV Flight Dynamics", In: 5th IUGRC International Undergraduate Research Conference, Military Technical College, Cairo, Egypt, pp. 541–547. Available at: https://journals.ekb.eg/article_246569_29de6e86b64658d034c77d-3dead8537f.pdf [Accessed: 01 May 2025]

Farhadi, R. M., Kortunov, V., Molchanov, A., Solianyk, T. (2018) "Estimation of the lateral aerodynamic coefficients for skywalker x8 flying wing from real flight-test data", Acta Polytechnica, 58(2), pp. 77–91. https://doi.org/10.14311/ap.2018.58.0077

Fatima, S. K., Abbas, S. M., Mir, I., Gul, F., Forestiero, A. (2023) "Flight Dynamics Modeling with Multi-Model Estimation Techniques: A Consolidated Framework", Journal of Electrical Engineering and Technology, 18(3), pp. 2371–2381. https://doi.org/10.1007/s42835-023-01376-4

Federal Aviation Administration (2021) "Maintaining Aircraft Control: Upset Prevention and Recovery Training", In: Airplane Flying Handbook, United States Department of Transportation, Federal Aviation Administration, Airman Testing Standards Branch, Oklahoma City, OK, USA, pp. 1–27. Available at: https://www.faa.gov/sites/faa.gov/files/regulations_policies/handbooks_manuals/aviation/airplane_handbook/06_afh_ch5.pdf [Accessed: 01 May 2025]

Gryte, K., Hann, R., Alam, M., Roháč, J., Johansen, T. A., Fossen, T. I. (2018) "Aerodynamic modeling of the Skywalker X8 Fixed-Wing Unmanned Aerial Vehicle", In: 2018 International Conference on Unmanned Aircraft Systems, ICUAS 2018, Dallas, TX, USA, pp. 826–835. https://doi.org/10.1109/icuas.2018.8453370

Jeong, H., Kim, S., Lee, Y-G., Cho, T., Jeong, J. (2024) "Aerodynamic Modeling and Verification of Quadrotor UAV Using Wind-Tunnel Test", International Journal of Aeronautical and Space Sciences, 25(3), pp. 809–835. https://doi.org/10.1007/s42405-023-00698-x

Juliawan, N., Chung, H-S., Lee, J-W., Kim, S. (2021) "Estimation and separation of longitudinal dynamic stability derivatives with forced oscillation method using computational fluid dynamics", Aerospace, 8(11), 354. https://doi.org/10.3390/aerospace8110354

Kamal, A., Aly, A. M., Elshabka, A. (2015) "Modeling and Simulation of Propeller Propulsion Model Using Wind Tunnel", In: AIAA Modeling and Simulation Technologies Conference, Kissimee, FL, USA,. AIAA 2015-1596. https://doi.org/10.2514/6.2015-1596

Kamal, A. M., Bayoumy, A. M., Elshabka, A. M. (2016) "Modeling and flight simulation of unmanned aerial vehicle enhanced with fine tuning", Aerospace Science and Technology, 51, pp. 106–117. https://doi.org/10.1016/j.ast.2016.01.022

Leishman, J. G. (2006) "Principles of Helicopter Aerodynamics", Cambridge University Press. ISBN 978-1107013353

Luckner, R. (2007) "Flugmechanik I Grundlagen und stationäre Flugzustände", Technische Universität Berlin, Germany.

Mahachi, A., Aloni, T., Mashevedze, L. (2022) "Unmanned Aerial Vehicle for Agriculture Surveillance", In: Aeronautics - New Advances, IntechOpen, 104476. https://doi.org/10.5772/intechopen.104476

makeflyeasy (2020) "Fighter Hand Throw". [online] Available at: https://en.makeflyeasy.com/index.php/fighter-hand-throw [Accessed: 27 December 2021]

Mateen, A., Krishna, B. V., Manoj, D.. (2024) "Advancements In UAV Wing Design : Aerodynamic Performance, Structural Integrity And Optimization Techniques", Journal of Mechanical and Civil Engineering, 21(6), pp. 34–37. https://doi.org/10.9790/1684-2106013437

Mi, B., Zhan, H. (2020) "Review of Numerical Simulations on Aircraft Dynamic Stability Derivatives", Archives of Computational Methods in Engineering, 27(5), pp. 1515–1544. https://doi.org/10.1007/s11831-019-09370-8

Moelyadi, M. A., Rohmahwati, Y. A. T., Nugraha, A. P. (2019) "CFD based determination of longitudinal static and dynamic stability derivatives of twin boom UAV", Journal of Applied Science and Engineering, 22(2), pp. 259–266. https://doi.org/10.6180/jase.201906_22(2).000

Mulder, J. A., van Stavaren, W. H. J. J., van der Vaart, J. C., de Weerdt, E., in 't Veld, A. C., Mooij, E. (2011) "Flight Dynamics", Lecture Notes, Delft University of Technology

Paz, C., Suárez, E., Gil, C., Vence, J. (2021) "Assessment of the methodology for the CFD simulation of the flight of a quadcopter UAV", Journal of Wind Engineering and Industrial Aerodynamics, 218, 104776. https://doi.org/10.1016/j.jweia.2021.104776

Priyambodo, T. K., Majid, A. (2021) "Modeling and Simulation of The UX-6 Fixed-Wing Unmanned Aerial Vehicle", Journal of Control, Automation and Electrical Systems, 32(5), pp. 1344–1355. https://doi.org/10.1007/s40313-021-00754-5

Pusztai, D., Lowenberg, M. H., Neild, S. A. (2024) "Flight Testing of a Dynamically Scaled Transport Aircraft Model for High-Alpha Wind Tunnel Data Validation", In: AIAA SCITECH 2024 Forum, Orlando, FL, USA, AIAA 2024-1497. https://doi.org/10.2514/6.2024-1497

Reinhardt, D., Gryte, K., Arne Johansen, T. (2022) "Modeling of the Skywalker X8 Fixed-Wing UAV: Flight Tests and System Identification", In: 2022 International Conference on Unmanned Aircraft Systems, ICUAS 2022, Dubrovnik, Croatia, pp. 506–515. https://doi.org/10.1109/icuas54217.2022.9836104

Sun, M., Duan, X., Qingling, L., Sun, C., Song, H. (2022) "Cost-Effectiveness analysis model for civil aircraft flight tests", Journal of Physics: Conference Series, 2336, 012021. https://doi.org/10.1088/1742-6596/2336/1/012021

Yechout, T. R., Morris, S. L., Bossert, D. E., Hallgren, W. F. (2003) "Introduction to Aircraft Flight Mechanics: Performance, Static Stability, Dynamic Stability, and Classical Feedback Control", American Institute of Aeronautics and Astronautic. Available at: https://ftp.idu.ac.id/wp-content/uploads/ebook/tdg/DESIGN%20SISTEM%20DAYA%20GERAK/Introduction%20to%20aircraft%20flight%20mechanics.pdf [Accessed: 27 December 2021]

Wu, Y., Liu, D., Wang, T., Zhao, A. (2023) "Research of a novel aerodynamic evaluation method for fixed-wing UAV", Journal of Physics: Conference Series, 2633, 0112001. https://doi.org/10.1088/1742-6596/2633/1/012001